RSC Advances

PAPER

View Article Online
View Journal | View Issue

Cite this: *RSC Adv.*, 2024, **14**, 16809

Photodissociation of leucine-enkephalin protonated peptide: an experimental and theoretical perspective†‡

Lara Martínez-Fernández, [a] Miloš Lj. Ranković, §[b] Francis Canon,[c] Laurent Nahon, [c] Alexandre Giuliani, [cd] Aleksandar R. Milosavljević *[c] and Ana Martin-Somer *[e]

Understanding the competing processes that govern far ultraviolet photodissociation (FUV-PD) of biopolymers such as proteins is a challenge. Here, we report a combined experimental and theoretical investigation of FUV-PD of protonated leucine-enkephalin pentapeptide ([YGGFL + H]$^+$) in the gas-phase. Time-dependent density functional theory (TD-DFT) calculations in combination with experiments and previous results for amino acids and shorter peptides help in rationalizing the evolution of the excited states. The results confirm that fragmentation of [YGGFL + H]$^+$ results mainly from vibrationally excited species in the ground electronic state, populated after internal conversion. We also propose fragmentation mechanisms for specific photo-fragments such as tyrosine side chain loss (with an extra hydrogen) or hydrogen loss. In general, we observe the same mechanisms as for smaller peptides or protonated Tyr and Phe, that are not quenched by the presence of other amino acids. Nevertheless, we also found some differences, as for H loss, in part due to the fact that the charge is solvated by the peptide chain and not only by the COOH terminal group.

Received 4th March 2024
Accepted 14th May 2024

DOI: 10.1039/d4ra01690d

rsc.li/rsc-advances

1. Introduction

The interaction of biomolecules with ultraviolet (UV) light is of paramount interest due to the pivotal role that such interactions play in fundamental biological processes,[1] ranging from DNA stability and repair[2–5] to protein function,[6–12] cellular signaling,[13,14] photosynthesis,[15,16] neurotransmission,[17] immune response,[18,19] or cell cycle regulation.[20]

In addition, the interaction of peptides with UV light has significant implications in many other fields such as the study of the origin of life,[21,22] photodegradation of industrially important polymeric materials[23,24] or photodegradation of biopharmaceuticals that can be exposed to UV light during their manufacturing and administration process.[25] Moreover, it is relevant in applications where the spectroscopic properties of the amino acid residues are applied. In this regard, the study of peptide-UV interactions becomes particularly significant in the context of mass spectrometry, where UV-induced fragmentation (UVPD, ultraviolet photodissociation) has attracted significant attention in the past years, since it is a proven and a powerful tool for structural elucidation, efficient for both small peptides and intact proteins with masses up to tens of thousands of Daltons.[26,27] Investigating UV-induced processes in gas-phase peptides allows assessing their intrinsic properties without the effects due to solvent, allowing to unravel the complexities of peptide electronic and vibrational dynamics.[28] It has also been suggested that gas-phase structure might be more appropriate to reproduce the biologically active geometry of peptide ligands in a hydrophobic environment than solution structures.[29]

For these reasons, ultraviolet and vacuum ultraviolet photodissociation as well as photoinduced dynamics of peptides have been extensively investigated in the past using both synchrotron radiation (SR) and lasers as well as from a theoretical point of view (see ref. 8–12, 28, 30–38 and references therein). In the far UV photon energy range (220–120 nm, or *c.a.* 5.5–10 eV) and below the ionization energy (IE), photodissociation is triggered by resonant electronic excitation of the target system, followed by competing relaxation pathways, such

[a]*Departamento de Química Física de Materiales, Instituto de Química Física de Materiales, Instituto de Química Física Blas Cabrera, CSIC, 28006, Madrid, Spain*
[b]*Institute of Physics Belgrade, University of Belgrade, Pregrevica 118, 11080 Belgrade, Serbia*
[c]*SOLEIL, l'Orme des Merisiers, St Aubin, BP48, F-91192 Gif sur Yvette Cedex, France*
[d]*INRAE, Dpet. Transform, UAR1008, Rue de la Géraudière, BP 71627, F-44316 Nantes, France*
[e]*Departamento de Química Física Aplicada, Universidad Autónoma de Madrid, Módulo 14, 28049, Spain. E-mail: ana.somer@uam.es*
† Correspondence and requests for materials should be addressed to A. M. S. and A. R. M.

‡ Electronic supplementary information (ESI) available. See DOI: https://doi.org/10.1039/d4ra01690d

§ Present address: Institute of Physical Chemistry J. 3Heyrovsky, CAS, Dolejškova 3, 18223 Prague 8, Czech Republic.

that UVPD can take place (i) directly from the excited state, or (ii) upon either radiative deexcitation or internal conversion (IC) into the vibrationally excited ground state (GS) where the ion subsequently fragments. Furthermore, there are two possible options prior to fragmentation in the GS: (a) the energy is redistributed statistically over many vibrational modes (intramolecular vibrational energy redistribution, IVR[39]) or it mostly remains in the vibrational modes of the excited bonds.[40] This highlights the complexity of peptide photofragmentation that is a combination of various competing processes.

Thus, a detailed description and understanding of the photofragmentation mechanisms offers valuable insights into the underlying photophysics of the deactivation process. However, unraveling these processes for a relatively large, isolated polypeptide remains challenging especially from a theoretical point of view[28] considering the large number of degrees of freedom associated with the size and floppiness of biopolymers. Some groups have studied deactivation mechanisms in proteins employing hybrid quantum mechanics/molecular mechanics (QM/MM) approaches where only a small region is treated at TD-DFT or higher theory level.[8–12] On the other hand, excited state relaxation mechanisms have been investigated in more detail for smaller systems such as *N*,*N*-dimethylformamide[41,42] (smallest molecule with a peptide bond); isolated neutral and protonated amino acids[43] (and references therein), related molecules such as substituted phenols,[44] iodotyrosine derivatives,[45] protonated adrenaline,[46] and small peptides such as dipeptides[31,38] tripeptides,[38,47] or phosphopeptides.[37] However, a comprehensive understanding of these processes for larger peptides has remained elusive.

In this context, we present a pioneering combined experimental and theoretical study on the resonant UV photodissociation of a gas-phase protonated pentapeptide: leucine-enkephalin (LeuEnk or YGGFL). LeuEnk is an endogenous opioid peptide found in the brain of animals, including humans, that acts as neurotransmitter. Among other functions, it plays a crucial role in pain modulation and nociception regulation in the body. LeuEnk has become a mass spectrometry standard,[48] and there is a plethora of papers having studied its fragmentation induced by different activation techniques, including collisional induced dissociation (CID)[48] and UV/VUV-induced fragmentation.[33,34,49–51] LeuEnk is a large enough molecule to be a good model for biologically important peptides and at the same time small enough (MH^+ = 556 Da) to be studied from a theoretical point of view.

In this article we aim to describe the intricate mechanisms involved in the deactivation processes at play at the molecular level in protonated LeuEnk after far ultraviolet (FUV) activation. To achieve this, we registered the FUV photodissociation mass spectra and we conducted a thorough TD-DFT study (CAM-B3LYP/cc-pVDZ). In particular, we have characterized the lowest-lying excited states in terms of nature, energies and intensities in the Franck–Condon (FC) region for $[YGGFL + H]^+$ precursor ion and, subsequently, mapped their possible relaxation mechanisms.

By integrating our findings with previous results on the excited state relaxation mechanisms of neutral and protonated Tyr and Phe amino acids, as well as protonated small peptides, we propose several deactivation pathways in competition. Some of these pathways lead to specific photofragments (such as H loss and Y + H side chain loss) not observed in CID experiments. This study contributes a unique perspective to the field, shedding light on the photochemical behavior of a biologically significant peptide in the gas phase under resonant FUV conditions.

2. Methods

2.1. Experimental

Singly protonated ions of bare LeuEnk were formed from an aqueous solution of the peptide using electrospray ionization (ESI). Mass and charge selected precursor was isolated and stored in a linear ion trap. The precursor ions were then irradiated by tunable synchrotron radiation (SR) in the 5.5–8.5 eV (*c.a.* 225–146 nm) photon energy range,[52,53] which is below the IE of protonatedLeuEnk reported at 8.9 eV.[33] Resonant photoexcitation of the target led to an increased ionic fragmentation *versus* non-resonant photon energy domain, which was recorded by mass spectrometry as a function of photon energy, *i.e.* by action spectroscopy.

2.1.1 Action spectroscopy. The experimental setup is based on a commercial Thermo Scientific LTQ XL mass spectrometer (LTQ), which was coupled to the VUV beamline DESIRS[54] at the synchrotron radiation facility SOLEIL (France), as described previously.[53] LTQ was equipped with nano electrospray ion source (NSI) on the front side. Water/MeCN (75 : 25 v/v) solution with LeuEnk molecules from Sigma Aldrich at a concentration of 10 μM was prepared and introduced into nano ESI as such, without further purification. A turbo pumping vacuum stage was used to accommodate pressure differences between beamline (10^{-8} mbar) and LTQ spectrometer (10^{-5} mbar). The pressure inside the ion trap is about 10^{-3} mbar due to helium buffer gas that is used to cool the ions and improve trapping. A home built supporting frame for LTQ allows for fine tuning the ion trap axis with respect to the photon beam, in order to obtain high signal to noise ratio. A mechanical shutter was designed and placed in the assembly with the vacuum stage to control the irradiation time.[55] Precursor cations, $[YGGFL + H]^+$, were isolated in the ion trap and subjected to VUV monochromatic photon beam during 500 ms. The tandem mass spectra (MS^2) were recorded as a function of the photon energy scanned in small steps of 0.2 eV from 5.7 eV to 8.5 eV. After the photon activation, ions were ejected and detected by two electron multiplier detectors with conversion dynodes (integral part of LTQ). Fragment ion yields, defined as the area under the peaks were extracted from recorded tandem mass spectra and normalized to the photon flux and total ionic current (or precursor ion intensity). The photon flux was measured separately under the same experimental conditions with photodiode (IRD, AXUV100) mounted in the vacuum stage assembly.

Collision induced dissociation (CID) experiments were conducted using the LTQ methods on the precursor ion. The nature of the fragment ion was assessed by the comparison of the m/z with theoretical values and by checking the isotopic ratio of the ions, from which the charge could be determined.

2.1.2 DESIRS beamline. The setup has been installed on a nonpermanent end station on the VUV beamline DESIRS at the SOLEIL storage ring (France).[54] The monochromatic VUV photon beam is delivered by an electromagnetic undulator OPHELIE2 (HU640 type), followed by a 6.65 m-long normal-incidence monochromator equipped with a low-dispersion (200 grooves mm^{-1}) grating. The latter provides a high photon flux of the order of 10^{12} to 10^{13} photons s^{-1} over the energy range used, within a photon bandwidth of typically 12 meV at 10 eV photon energy with 200 mm exit slit. It is important to note that higher harmonics of the undulator are cut off by a gas filter filled with Kr in the 7 to 8.5 eV and by a SUPRASIL window in the 5.5 to 7.2 eV.

2.2. Computational details

Density functional theory (DFT) and its Time-Dependent version (TD-DFT) together with cc-pVDZ basis set were used to optimize the ground state (GS) minimum of LeuEnk, characterize the excited state (ES) at this geometry and their potential energy surfaces (PES), respectively. We assessed the performance of different functionals and basis set (see Fig. S2 and S3‡). In particular, the CAM-B3LYP[56] functional was selected, due to its good performance in treating such kind of extended π systems.[12,57,58]

To simulate the vertical absorption spectrum, we computed the vertical absorption energies (VAEs) and oscillator strengths (f) for the 100 lowest ES. For an easier comparison with the experimental spectra, each VAE was shifted by -0.35 eV and a phenomenological broadening was used by adding a Gaussian with half width half maximum of 0.2 eV. This shift accounts for all different sources of approximations in our calculations (functional, incomplete basis set, lack of vibronic and thermal effects).[59] TD-DFT absorption energies are typically blue-shifted compared to experimental absorption spectra. For small or medium-size molecules allowing the use of large basis set, the error is ~0.2–0.3 eV,[58] although it can be larger when the basis set is reduced.

The characterization of the ES nature in such complex systems is not straightforward since, usually, they are a mixture of different states and furthermore the molecular orbitals are delocalized along the molecule. Excited-ground state density difference provides a good alternative because it shows from where the density moves when populating a given excited state, being, then, very useful. Throughout this manuscript the color code is that the electron density moves from the blue region (negative density difference) of the molecule to the green areas (positive density difference). All the above calculations were performed with the Gaussian 16 suite of programs.[60]

We also performed the analysis of the non-covalent interactions (NCI) plots, using NCI code.[61,62] NCI plots allow to visualize the different non-covalent interaction regions using a color code to rank those interactions. Red is used for destabilizing interactions, blue for stabilizing interactions and green for delocalized weak interactions. The intensity of these colors is associated with the interaction strength.

3. Results and discussion

3.1. Protonated leucine-enkephalin structure

The sequence for protonated LeuEnk is shown in Fig. 1 together with the backbone fragments named following Biemann's nomenclature.[63] The 3D structure for GS $[YGGFL + H]^+$ was elucidated by Burke *et al.*[64] combining IR-UV double resonance spectroscopy of cryogenically cooled protonated LeuEnk with DFT calculations (M052X/6-31+G(d)). We re-optimized that geometry at CAM-B3LYP/cc-pVDZ level of theory used to describe the photodissociation of protonated LeuEnk. The optimized structure is shown in Fig. 1 together with the NCI isosurface.

As we can see in Fig. 1, the proton is located on the N-terminal amino group, which is the most basic site. There is a net of H-bonds keeping the peptide in a hairpin like structure. These bonds are revealed by the blue (strong attractive interaction) flat circular regions of the NCI plots (marked with pink arrows in Fig. 1). In the 3D structure we can observe that the positive charge in the nitrogen is solvated by H bonds formed with (i) the carbonyl groups of the 3rd peptide backbone and (ii) the C-terminal COOH.

3.2. Photofragmentation spectra

Fig. 2 shows tandem mass spectra (MS^2) of protonated LeuEnk, at the resonant photon activation energy of 6.7 eV together with the CID spectra for comparison.

The fragmentation pattern of $[YGGFL\text{-}H]^+$ after UV light irradiation (Fig. 2a) is dominated by the backbone fragments a_4, b_4, b_3 and y_2, as well as internal ions and neutral losses, mainly water. As already pointed out,[34] the fragmentation pattern of protonated LeuEnk below ionization energy appears very similar to that produced by CID (Fig. 2b), suggesting that upon electronic excitation, IC to a vibrationally hot GS is the dominant deactivation mechanism. Photo-specific fragments like Y and F side chain losses (m/z 448, and 465, respectively) usually observed in photofragmentation of peptides containing these amino acids are also present in the FUV-PD spectrum. H loss (m/z 555), another specific photofragment, is also observed. The presence of these fragments suggests a competition between fragmentation directly from the ES and fragmentation from a vibrationally hot GS after IC.

3.3. Photoabsorption spectra

3.3.1 Experimental. Fig. 3 shows measured action photoabsorption spectra of $[YGGFL + H]^+$, obtained as total ion yields (TIYs) over all resolved fragments in the photon energy range 5.5–8.5 eV. The absorption maximum is at about 6.7 eV. Except for the later result,[34] we are not aware of any other reported gas-phase absorption measurements for protonated LeuEnk in this photon energy region, since laser experiments are performed at quasi-discrete energies or within rather small range in the near/mid-UV by using optical parametric oscillator (OPO),[50,51] while SR data are reported at higher energies.[33] Solution-phase UV-Vis spectra cannot reach the present energy range owing to the strong VUV absorption of the solvents.[51] The photofragment

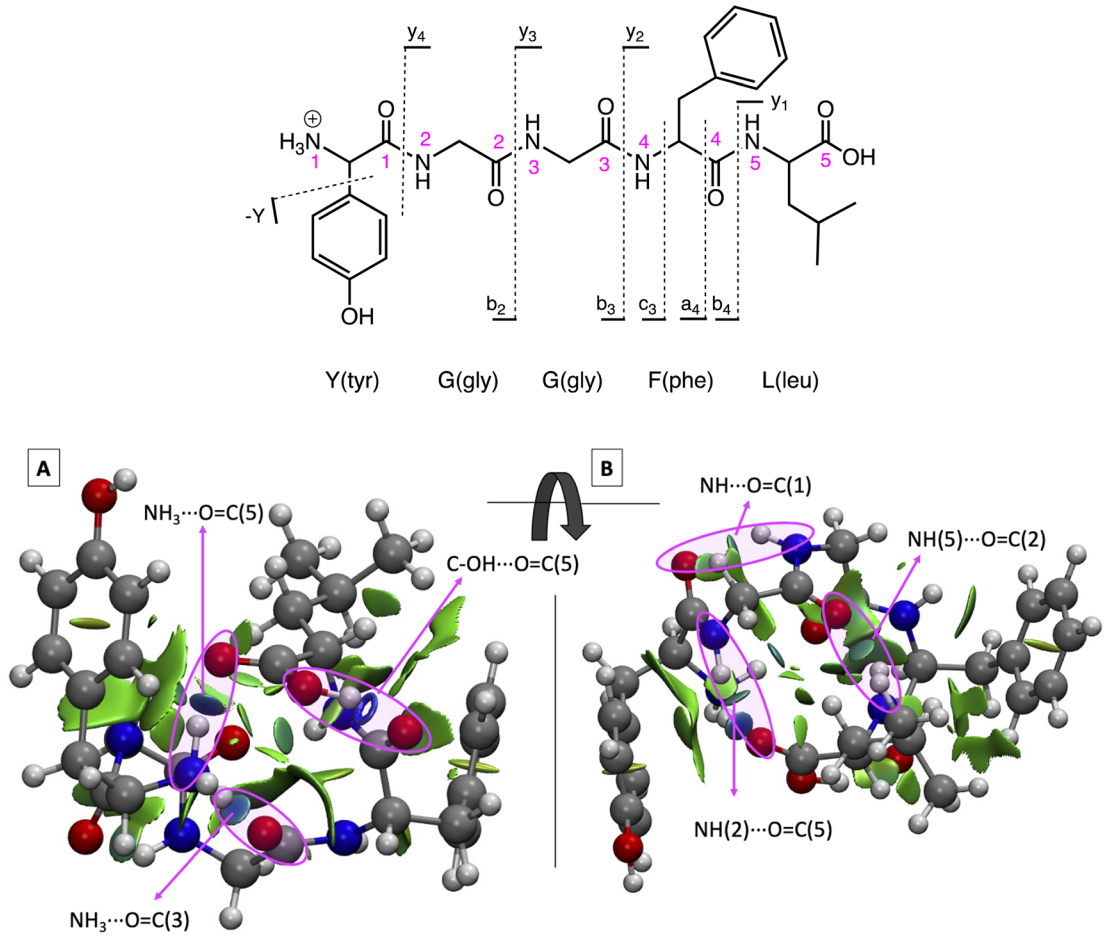

Fig. 1 (Top) Protonated LeuEnk, $[YGGFL + H]^+$, schematic structure together with the backbone fragments named following Biemann's nomenclature.[63] (Bottom) Optimized 3D structure showing the NCI plots for the ground state minimum, min0. (A) and (B) are two different views of the same structure. Pink arrows point the NCI surfaces corresponding to the H-bonds.

partial ion yields (PIY) for some selected fragments are shown in Fig. S1.‡ All of them (but water loss) show similar behavior with a maximum around 6.5–6.8 eV. The water loss channel shows a monotonic decrease with increasing photon energy up to ~8 eV where there is 0 relative intensity.

3.3.2 Theoretical. The calculated absorption spectra obtained from optimized protonated LeuEnk structure (Fig. 1) is shown in Fig. 3 together with the experimental spectrum. The computed spectrum of $[YGGFL + H]^+$ is characterized by a main absorption band with a maximum at ~6.7 eV that is flanked by a small band peaking about 5.5 eV plus a shoulder at ~8 eV. In order to characterize the main electronic transitions responsible for the absorption maxima we selected the brightest ES ($f > 0.05$) in the FC region up to 8 eV and plotted their corresponding electronic density difference. This corresponds to 22 ES. The first six ES (S_1–S_6) where also studied even if $f < 0.05$ for these states (see Table S1‡). The FC region refers to the region of the PES defined by the GS minimum of the molecule (see Section S1.1‡ for an extended explanation). This analysis shows that all the ES can be classified within six main families as following. F1/F2: electronic transition localized at the phenol ring (Y side chain) and phenyl ring (F side chain). F3/F4/F5: electron density moves towards the peptide backbone from the phenyl/phenol/both groups and F6: electron density moves from phenyl and phenol rings towards the C-terminal carboxylic acid. Fig. 4 shows an example of the electron density difference for each family.

3.3.3 Comparison. There is a good comparison between experimental and computed absorption spectra with a slightly more pronounced difference in the highest energy region, 8.4 eV (Fig. 3). However, when comparing both spectra, it should be taken into account that they are not exactly equivalent. Using TD-DFT we simulate the molecule's absorption spectrum, while experimentally, it is not possible to measure the attenuation of the beam through the trapped ions owing to the low density of the gaseous species. Therefore, the experimental spectrum shown is not the absorption spectrum but is obtained as the sum of total ion yields produced by dissociation of the precursor ions, which may reflect at least partially the photoabsorption spectra. Fragments below the cutoff mass at m/z 150 are not included in the generation of the experimental spectrum. Possible radiative decay cannot be detected either in the present experiment. Nevertheless, it has been observed that fluorescence becomes less important as the peptide size increases.[28,65,66] All these factors may affect the comparison with the computed spectrum.

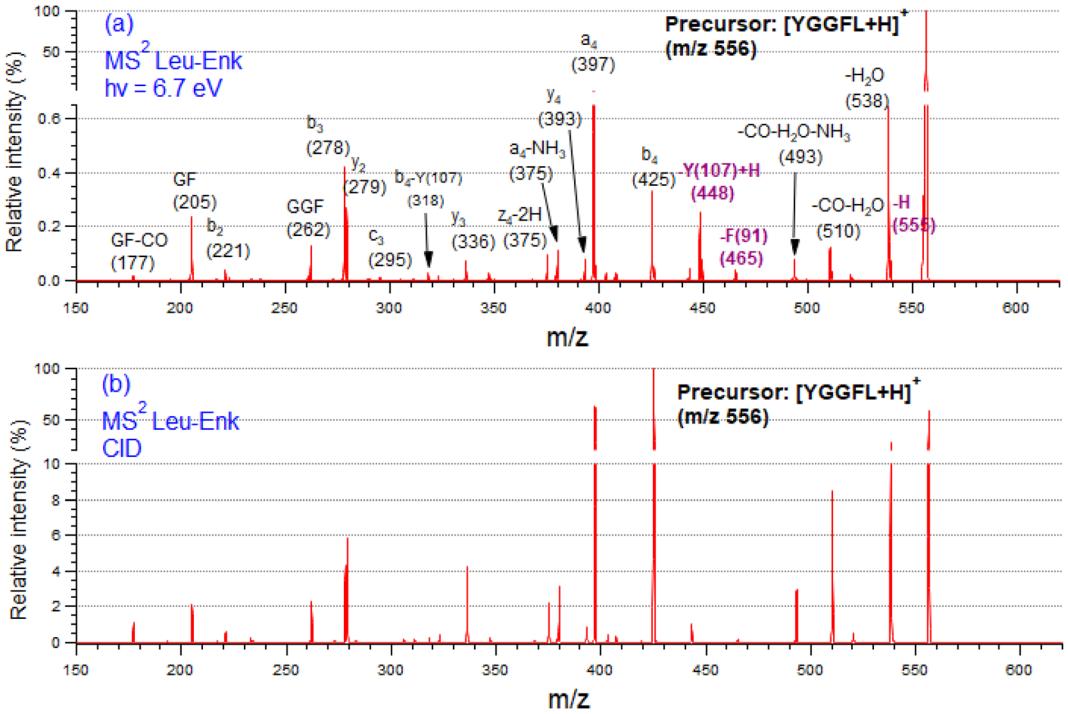

Fig. 2 Tandem mass spectra (MS^2) of protonated leucine-enkephalin peptide recorded (a) at the photon energy of 6.7 eV and (b) collision induced dissociation spectrum. The assignment of the fragments is given in the figure.

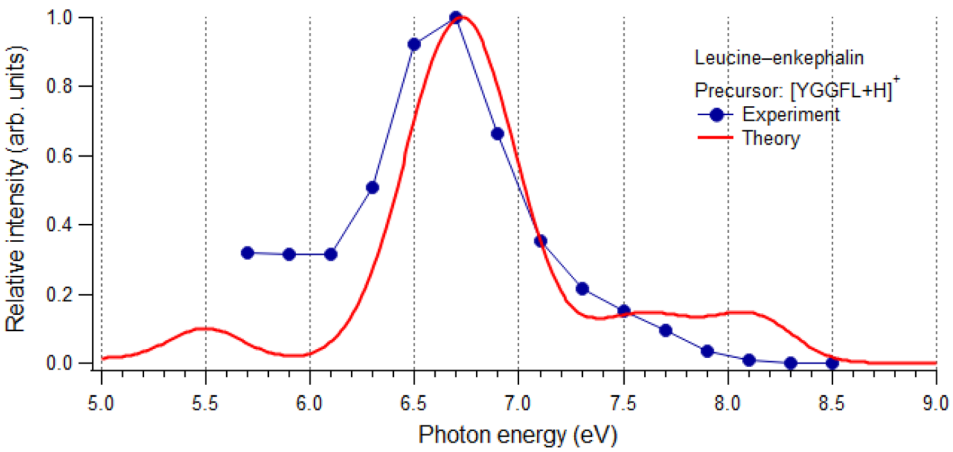

Fig. 3 The experimental total ion yield, obtained as the sum over all resolved fragments in the *m*/*z* 150–620 range, compared to the normalized calculated absorption spectra (TD-CAM-B3LYP/cc-pVDZ).

3.4. Photodissociation mechanisms

Since the experimental spectrum (recall Fig. 2a) shows specific photo-fragments (*m*/*z* 555, H loss; *m*/*z* 448 Y side chain loss + H and *m*/*z* 465 F side chain loss), we mapped the possible relaxation mechanisms from the FC region by optimizing the selected brightest ES (Table S2‡ contains additional information). The optimizations lead to seven different minima on the S_1 surface plus one minimum in the S_2 ES. Similarly to the FC region, the types of S_1 minima can also be classified according to where the electron density is localized. The geometry and electronic density difference of each of these minima is shown in Fig. 5. In all of them, the electronic density is localized on the X peptide bond (min-PBX), on the aromatic ring of the Y or F side chains, or in the COOH (min-HT: one H of the N-terminal NH_3^+ is transferred to the C-terminal). Min1-HT is the most stable minimum by far (more than 1 eV). The relative energies of the other minima are within a 0.5 eV range.

Given the high density of excited states accessible in the FC region and minima found in the S_1 surface, and in the absence of a dynamic study, we have attempted to estimate which minimum is more likely to be populated. With this objective, we define the quantity % f_{ave}. To compute % f_{ave} we assigned the

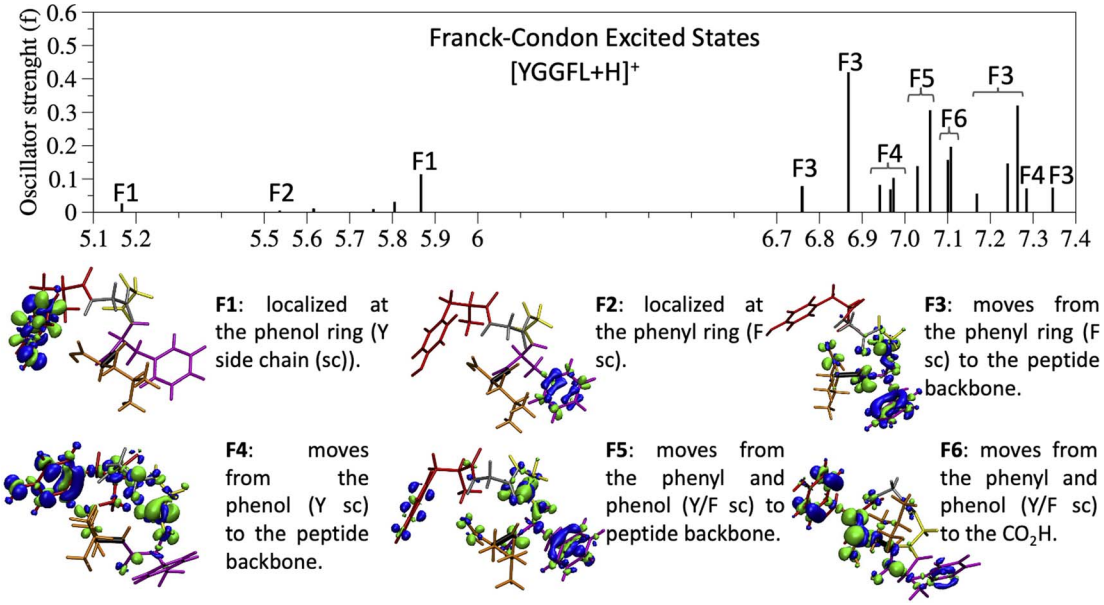

Fig. 4 Brightest excited states (oscillator strength $f > 0.05$) up to 8 eV and description of the families used to classify the excited states at the Franck–Condon region with an example of the electron density difference for each family showing how the electron density changes when going from the ground to the excited state. The family of each excited state is indicated on the graph.

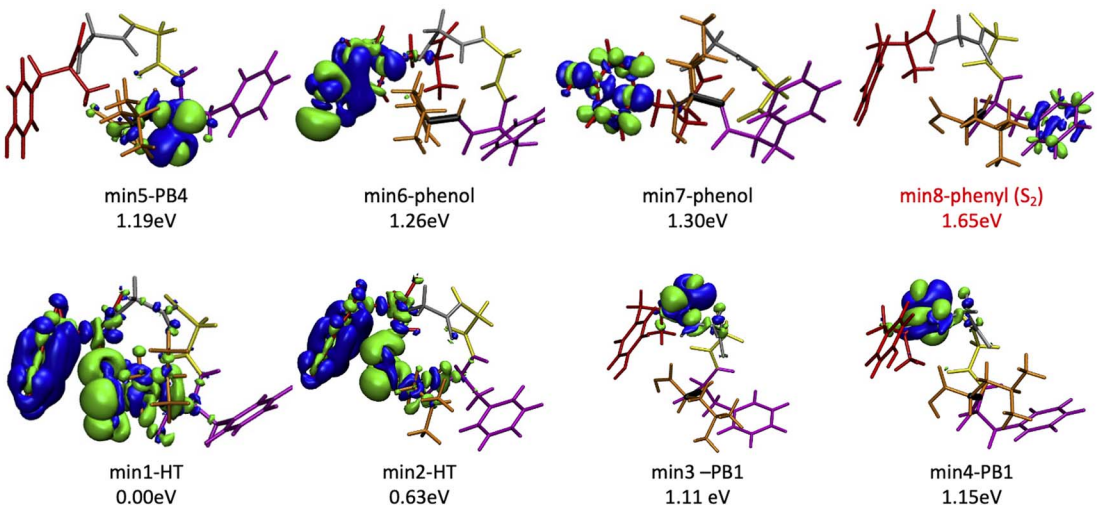

Fig. 5 Optimized geometries, electron density differences and relative energies for the S_1 and S_2 minima.

value 100% to the oscillator strength of the brightest state at the FC region (S_{16} with $f = 0.42$) and computed the corresponding percentage, relative to this maximum, for each of the states. Then we calculated the average of the % f of all the states leading to a given minimum. Thus, the highest the % f_{ave}, the brightest are the states leading to that minimum. The computed values are shown in Table 1 together with other quantities like number of states leading to each minimum and the oscillator strength of the brightest of those minima. From the values of % f_{ave} (Table 1) we expect min1-HT to be the most populated, since the most intense FC bright states lead to this minimum and the larger number of states (six). Furthermore, it is the most stable S_1 minimum by far (>1 eV). After min1-HT, min5-PB4 and min6-phenol will be the second most populated being 1.19 and 1.26 eV higher in energy than min1-HT. We will discuss possible deactivation mechanism from these minima.

Previous studies have shown that some fragmentation channels could proceed through triplet states.[67,68] To preliminary assess the possibility of intersystem crossing (ISC) from these minima we have estimated the spin orbit coupling (SOC) terms using the single particle Breit–Pauli operator with an effective charge approximation as implemented in the PySOC code.[69] The values for the SOC and vertical energies computed at each S_1 minima are reported in Tables S2–S10 of the ESI.‡ For the minima with large values of SOC (min3, min4, min5, and

Table 1 Excited state minima for [YGGFL + H]$^+$. Relative energies of each minimum, number of states that reach the minimum after optimization (#states), average weight of the oscillator strength at the FC region of the state reaching the minimum (% f_{ave}), f_{max} for the brightest state of each group, and vertical energy to the GS for each minimum. Marked in bold are the 3 more important ones

Minimum	Rel. E [eV]	#States	% f_{ave}	f_{max}	Vert. E [eV]
Min1-HT	**0.00**	**6**	**43**	**0.42**	**0.99**
Min2-HT	0.63	1	20	0.08	2.19
Min3-PB1	1.11	4	9	0.11	3.75
Min4-PB1	1.15	1	17	0.07	3.75
Min5-PB4	**1.19**	**5**	**36**	**0.32**	**3.67**
Min6-phenol	**1.26**	**1**	**35**	**0.15**	**1.00**
Min7-phenol	1.30	2	7	0.06	4.82
Min8-phenyl	1.65	2	2	0.07	5.19

min6) we then optimized the T_1 state reaching in all cases to a T_1 minimum (Table S11‡). In all the cases we observe small conformational rearrangement and no structural changes suggesting a fragmentation process originating from these structures, with the only exception of min6 (*vide infra*). In particular, there is no sign of C_α–C_β bond weaking at any of the studied T_1 minimum. In all of them C_α–C_β bond distance is 1.54 Å, exactly the same value as in the GS minimum, min0.

3.4.1 Min1-HT. We explored the characteristics of min1-HT in further details (we did not consider min2-HT since it is similar in nature to min1-HT). In min1-HT, a proton from the protonated ammonium is transferred to the carboxylic oxygen of the C-terminal COOH group (Excited State Proton Transfer, ESPT). This means that there is no barrier from the FC region for the proton transfer leading to min1-HT (Scheme 1). From this minimum, it could be observed CO + H_2O loss (m/z 510) and H_2O loss (m/z 538) channels. However, these are also typical fragments observed in CID fragmentation. Taking into account that the vertical energy of min1-HT is small (0.99 eV), we can also expect this state to deactivate to the GS surface. However, in the GS this structure is not a minimum so the molecule will evolve yielding H_2O loss and CO + H_2O loss or the now activated H^+ will jump to the different basic positions on the peptide backbone, triggering fragmentation as proposed by the mobile-proton model[70] usually employed to explain CID fragmentation. Similar ESPT mechanisms have also been previously evoked to rationalize the photophysics of protonated aromatic amino acids and derivatives such as short peptides and neurotransmitters.[43,46,65,71,72] It has also been used to explain the CO + H_2O loss channel throughout H^+ transfer from NH_3^+ to COOH.[43,72]

3.4.2 Min-phenol. Notice there are two different min-phenol. The most stable one, min6-phenol, 1.26 eV above min1-HT, with electron density resembling the $\pi\sigma^*$ dissociative state used to explain nonradiative decay of neutral aromatic amino acids.[73] This state shows a repulsive potential-energy function with respect to the OH stretching proposed to be responsible for H loss from phenol. Indeed, min6 shows a large phenol's O–H distance (1.696 Å). This minimum also presents a large value of SOC with T_1 (26 cm^{-1}) (see Table S8‡). In view of the calculated SOC we cannot discard the population of triplet states from these region of the PES. Therefore, we optimized this structure in T_1 PES, reaching a minimum with O–H distance even larger, 2.591 Å. A relaxed scan of the OH distance in T_1 PES shows that H loss along the triplet is a barrierless process (see Fig. S4 of ESI‡). Taking this into account we hypothesize that the H loss proceeds *via* T_1 state with the H coming from the phenol ring of Tyr side chain (Scheme 2). On

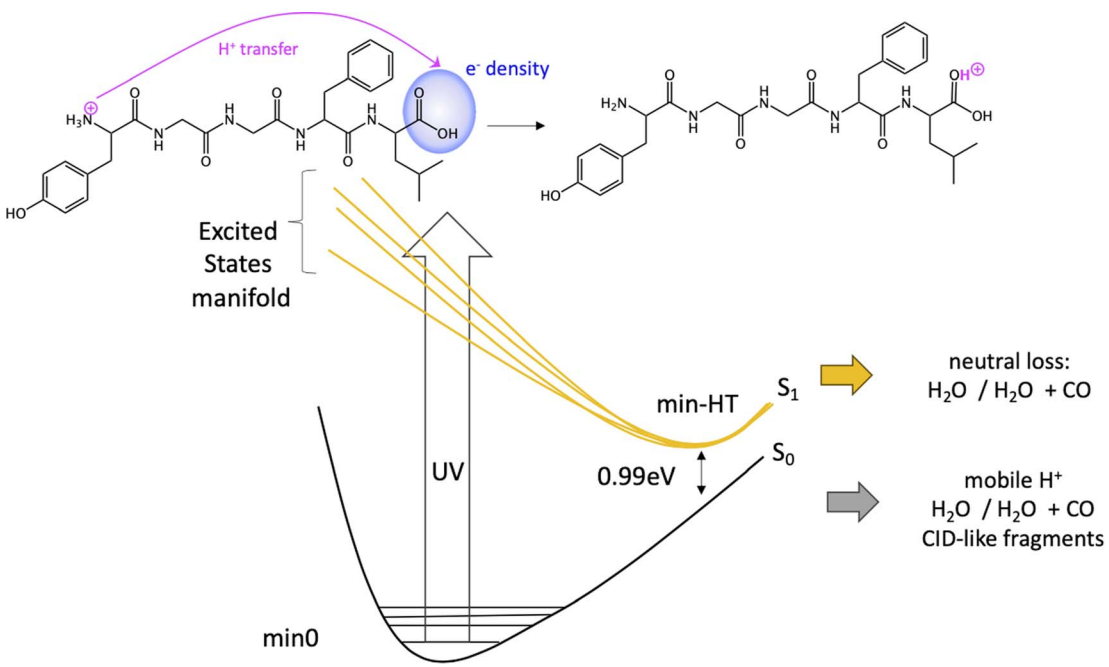

Scheme 1 Fragmentation mechanisms from min-HT.

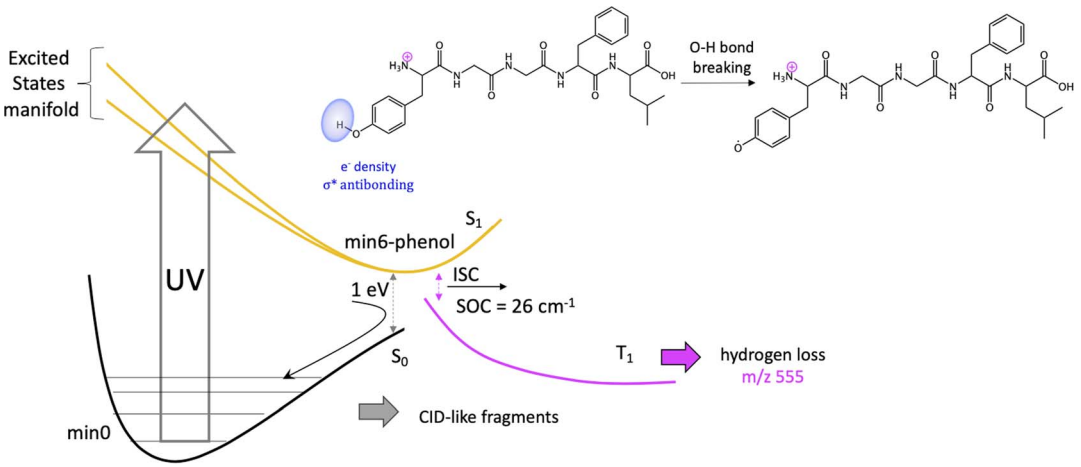

Scheme 2 Fragmentation mechanism from min6-phenol.

the other hand, the vertical energy from min6 (S_1) to S_0 PES is ~1 eV what could lead to IC to a vibrationally hot GS eventually followed by fragmentation. We expect the two deactivation pathways, H loss and GS fragmentation, to be in competition.

It should be noticed that the mechanisms proposed to explain H loss from charged amino acids as $TyrH^+$ or short, charged peptides, is different to the one we proposed here for protonated LeuEnk, since in the other cases the lost H comes from the charged NH_3^+ group.[43,72] This can be explained by the high sensitivity of the nonradiative deactivation processes to the backbone environment of the aromatic ring. Considering protonated LeuEnk geometry, where the peptide chain is long enough to allow the peptide to fold in such a way that the NH_3^+ charge is solvated by COOH group and the carbonyl groups of two peptide bonds (recall Fig. 1), the phenol environment resembles more of the neutral tyrosine than of protonated Tyr or small protonated peptides containing Tyr, where the NH_3^+ group is interacting with the electronic cloud of the ring. Thus, it is logical that the H loss mechanism resembles more that proposed for neutral aromatic amino acids.[73]

The other minimum, min7-phenol, is slightly higher in energy (1.30 eV). The excess of electronic density (green surface) of the min7-phenol resembles the $\pi\pi^*$ state proposed to explain fragmentation for protonated Tyr and Phe[43] and the neurotransmitters noradrenaline[71] and adrenaline.[46] The proposed mechanism implies an ESPT from the ammonium to the aromatic ring (of Tyr in this case), followed by C_α–C_β bond breaking, with the corresponding fragment (Y side chain) bearing an extra hydrogen as compared to the mass of the aromatic chromophore cation, *i.e.*, a mass difference with MH^+ of 108 instead of 107. This mechanism will lead to the observation of the photofragment *m*/*z* 448 (Scheme 3).

A similar mechanism will be in place to explain F side chain loss (*m*/*z* 465). However, it is worth to note that the minima with electron density localized at the F side chain (min8-phenyl) is the highest in energy and belongs to the S_2 surface. In addition, it has the lowest value of % f_{ave} (only 2 excited states, with very low oscillator strength, lead to this minimum). This is consistent with the low intensity observed for this channel.

3.4.3 Min5-PB4. The other S_1 minimum that we expect to be significantly populated is min5-PB4 (1.19 eV) with a vertical energy of 3.67 eV, thus we do not expect this minimum to deactivate rapidly to the GS surface by IC. In this S_1 minimum the electronic density moves towards the carbonyl of the 4th peptide bond. This

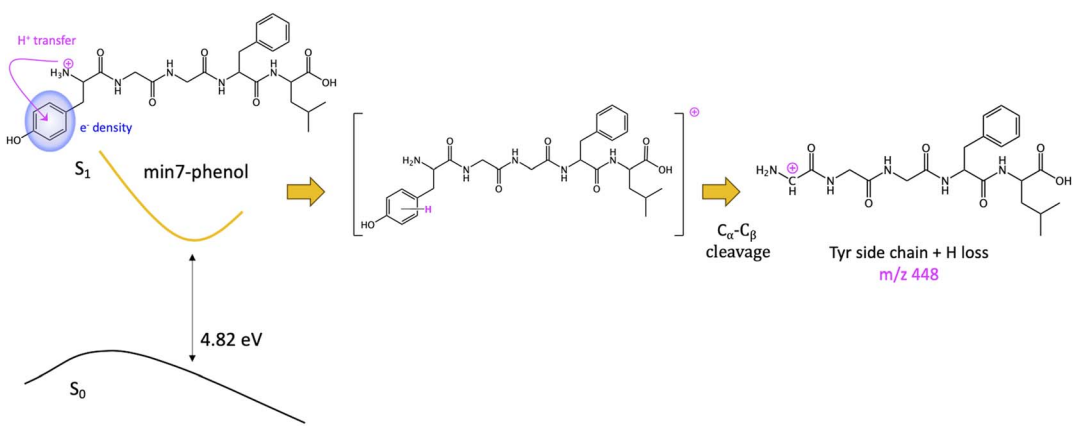

Scheme 3 Fragmentation mechanism from min7-phenol.

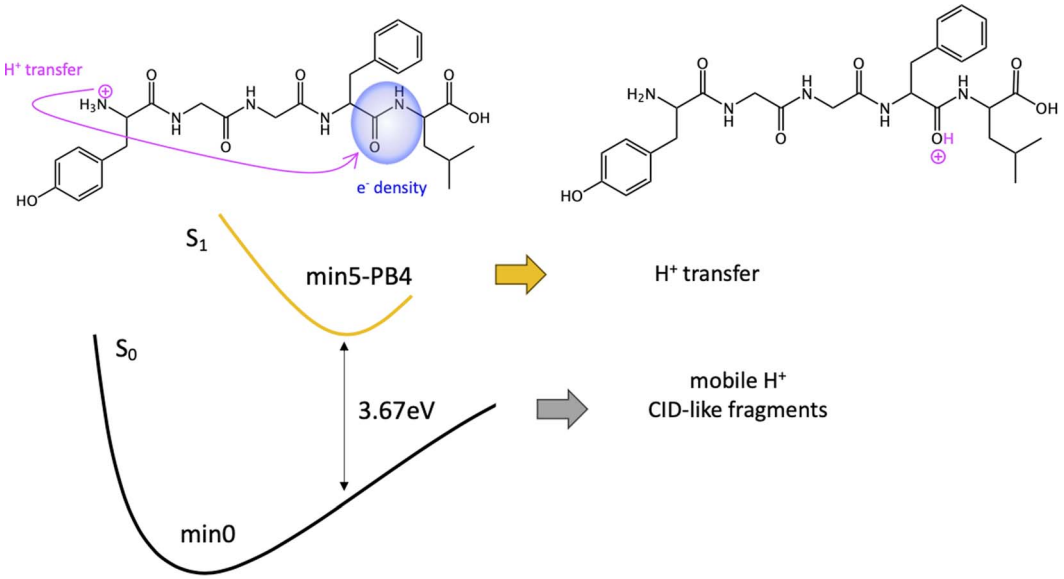

Scheme 4 Fragmentation mechanisms from min5-PB4.

could trigger a proton transfer to the carboxylic oxygen weakening the amide bond and eventually leading to b_4/a_4 fragments (a_4 generates by CO loss from b_4 fragment) (Scheme 4). These fragments are also observed in CID.

4. Conclusions

In conclusion, we have performed a combined experimental and theoretical study of FUV-PD of a protonated pentapeptide, leucine-enkephalin, isolated in the gas-phase. TD-DFT calculations were performed to investigate in detail excitation of $[YGGFL + H]^+$ and the evolution of the excited states.

Calculations suggest that the main fragmentation mechanism starts by an electron transfer from the aromatic ring of Y/F side chain to the carboxylic acid, rapidly followed by a barrierless excited state proton transfer (ESPT) from the NH_3^+ terminal to the COOH forming min-HT. From this minimum, CO and CO + H_2O loss could be observed. Also, IC to the GS could take place, where the activated H^+ can move to the different basic positions on the peptide backbone triggering fragmentation as proposed by the mobile-proton model usually employed to explain CID fragmentation.

We also proposed a mechanism for the specific photofragments. In the singlet PES, the channel leading to the photofragment *m*/*z* 448 (loss of Tyr side chain + H), would be triggered by an ESPT to Tyr aromatic ring driven by a light-induced electron transfer to the aromatic ring and followed by C_α–C_β bond cleavage. Another relevant channel would be the light-induced electron transfer from the aromatic ring (F/Y residues) to the carbonyl of the 4th peptide bond. This charge transfer might trigger a proton transfer from the ammonium group to the negatively charged CO followed by fragmentation at this amide bond (b_4/a_4 ions). Nevertheless, this will lead to the same fragments as in CID experiments.

On the other hand, since some of the singlet minima present large SOC, and therefore triplet population cannot be discarded, we complete the study considering possible photofragmentation mechanisms in the triplet manifold. However, the T_1 minima optimized from this region of the PES show small structural changes but for min6, leading to H loss. For this channel, calculations suggest that the H is lost from phenol's hydroxyl group of Tyr sice chain, as observed for the neutral peptide and in contrast with mechanism proposed for protonated Tyr. H loss in T_1 PES is a barrierless process.

In summary, the fragmentation mechanisms proposed are mostly triggered by ESPT followed by (i) fragmentation in the excited state (Y + H side chain loss, H loss) or (ii) IC to a hot vibrationally GS where fragmentation takes place. The resemblance of FUV-PD and CID mass spectra support the assumption that the fragmentation mainly takes place from a vibrationally hot peptide in the GS as it happens in CID. Despite the initiation of the process through photon absorption rather than collisions, it is ultimately the proton transfer that triggers fragmentation. Previous studies have already pointed out the validity of the mobile proton model to explain UVPD results.[74,75] If, following UV photon absorption, there is a charge transfer to the CO groups of peptide backbone with subsequent proton migration (ESPT), the final observed fragments will be the same as in a CID-like mechanism. However, when aromatic amino acids are present, proton might migrate to the side chain aromatic ring of these amino acids *via* ESPT, leading to the observation of specific photofragments (C_α–C_β bond breaking) that do not appear in CID experiments.

The present work deepens the existing understanding of the complex cascading processes that govern photodissociation of a quite large biopolymer in the far ultraviolet range.

Author contributions

A. M., A. G. and L. N. conceived and design the experiment. A. R. M., M. R., A. G., F. C. and L. N. conducted the measurements.

A. R. M. and M. R. treated the experimental data. A. M. S. and L. M. F. designed the theoretical study and performed and analyzed TD-DFT calculations. A. M. S., L. M. F. and A. R. M. co-wrote the first draft of the paper, which was then commented, corrected and improved by all coauthors.

Conflicts of interest

The authors declare no conflict of interest.

Acknowledgements

We thank the technical staff of SOLEIL for running smoothly the facility under project No. 20131031. AMS acknowledges Madrid Government (Comunidad de Madrid-Spain) under the Multiannual Agreement with UAM in the line Support to Young Researchers, in the context of the V PRICIT (SI3-PJI-2021-00463) and CCC-UAM for generous allocation of computing time. MR acknowledges support from the Ministry of education, science and technological development of Republic of Serbia under the grant OI 171020. AG acknowledges support from the Agence Nationale de la Recherche Scientifique, France, contract grant number: ANR-08-BLAN-0065. The collaborative work was performed within the framework MD-GAS CA18212 COST action. We are grateful to Ines Corral for discussions and help with calculations.

References

1 D. I. Pattison and M. J. Davies, *Actions of Ultraviolet Light on Cellular Structures*, Springer, New York, 2006.
2 R. P. Rastogi, Richa, A. Kumar, M. B. Tyagi and R. P. Sinha, Molecular mechanisms of ultraviolet radiation-induced DNA damage and repair, *J. Nucleic Acids*, 2010, **2010**, 1–32.
3 *DNA Photodamage: from Light Absorption to Cellular Responses and Skin Cancer*, ed. R. Improta and T. Douki, The Royal Society of Chemistr, 2021.
4 J. S. Taylor, Unraveling the Molecular Pathway from Sunlight to Skin Cancer, *Acc. Chem. Res.*, 1994, **27**, 76–82.
5 L. Martínez Fernández, F. Santoro and R. Improta, Nucleic Acids as a Playground for the Computational Study of the Photophysics and Photochemistry of Multichromophore Assemblies, *Acc. Chem. Res.*, 2022, **55**, 2077–2087.
6 V. A. Bahamondes Lorca and S. Wu, Ultraviolet Light, Unfolded Protein Response and Autophagy, *Photochem. Photobiol.*, 2023, **99**, 498–508.
7 D. I. Pattison, A. S. Rahmanto and M. J. Davies, *Photochem. Photobiol. Sci.*, 2012, **11**, 38–53.
8 G. Giuliani, F. Melaccio, S. Gozem, A. Cappelli and M. Olivucci, QM/MM Investigation of the Spectroscopic Properties of the Fluorophore of Bacterial Luciferase, *J. Chem. Theory Comput.*, 2021, **17**, 605–613.
9 L. V. Schäfer, G. Groenhof, A. R. Klingen, G. M. Ullmann, M. Boggio-Pasqua, M. A. Robb and H. Grubmüller, Photoswitching of the fluorescent protein asFP595: Mechanism, proton pathways, and absorption spectra, *Angew. Chem., Int. Ed.*, 2007, **46**, 530–536.
10 D. Polli, P. Altoè, O. Weingart, K. M. Spillane, C. Manzoni, D. Brida, G. Tomasello, G. Orlandi, P. Kukura, R. A. Mathies, M. Garavelli and G. Cerullo, Conical intersection dynamics of the primary photoisomerization event in vision, *Nature*, 2010, **467**, 440–443.
11 S. Gozem, P. J. M. Johnson, A. Halpin, H. L. Luk, T. Morizumi, V. I. Prokhorenko, O. P. Ernst, M. Olivucci and R. J. D. Miller, Excited-State Vibronic Dynamics of Bacteriorhodopsin from Two-Dimensional Electronic Photon Echo Spectroscopy and Multiconfigurational Quantum Chemistry, *J. Phys. Chem. Lett.*, 2020, **11**, 3889–3896.
12 P. Nogly, T. Weinert, D. James, S. Carbajo, D. Ozerov, A. Furrer, D. Gashi, V. Borin, P. Skopintsev, K. Jaeger, K. Nass, P. Båth, R. Bosman, J. Koglin, M. Seaberg, T. Lane, D. Kekilli, S. Brünle, T. Tanaka, W. Wu, C. Milne, T. White, A. Barty, U. Weierstall, V. Panneels, E. Nango, S. Iwata, M. Hunter, I. Schapiro, G. Schertler, R. Neutze and J. Standfuss, Retinal isomerization in bacteriorhodopsin captured by a femtosecond x-ray laser, *Science*, 2018, **361**, eaat0094.
13 C. López-Camarillo, E. A. Ocampo, M. L. Casamichana, C. Pérez-Plasencia, E. Álvarez-Sánchez and L. A. Marchat, Protein kinases and transcription factors activation in response to UV-radiation of skin: Implications for carcinogenesis, *Int. J. Mol. Sci.*, 2012, **13**, 142–172.
14 A. Gęgotek, S. Atalay and E. Skrzydlewska, UV induced changes in proteome of rats plasma are reversed by dermally applied cannabidiol, *Sci. Rep.*, 2021, **11**, 20666.
15 L. Vanhaelewyn, D. Van Der Straeten, B. De Coninck and F. Vandenbussche, *Front. Plant Sci.*, 2020, **11**, 597642.
16 S. Kataria, A. Jajoo and K. N. Guruprasad, Impact of increasing Ultraviolet-B (UV-B) radiation on photosynthetic processes, *J. Photochem. Photobiol., B*, 2014, **137**, 55–66.
17 A. T. Slominski, M. A. Zmijewski, P. M. Plonka, J. P. Szaflarski and R. Paus, How UV Light Touches the Brain and Endocrine System Through Skin, and Why, *Endocrinology*, 2018, **159**, 1992–2007.
18 P. H. Hart, S. Gorman and J. J. Finlay-Jones, Modulation of the immune system by UV radiation: More than just the effects of vitamin D?, *Nat. Rev. Immunol.*, 2011, **11**, 584–596.
19 J. J. Bernard, R. L. Gallo and J. Krutmann, Photoimmunology: how ultraviolet radiation affects the immune system, *Nat. Rev. Immunol.*, 2019, **19**, 688–701.
20 S. Takeuchi, T. Matsuda, R. Ono, M. Tsujimoto and C. Nishigori, Mitotic genes are transcriptionally upregulated in the fibroblast irradiated with very low doses of UV-C, *Sci. Rep.*, 2016, **6**, 29233.
21 O. Licht, D. Barreiro-Lage, P. Rousseau, A. Giuliani, A. R. Milosavljević, A. Isaak, Y. Mastai, A. Albeck, R. Singh, V. T. T. Nguyen, L. Nahon, L. Martínez-Fernández, S. Díaz-Tendero and Y. Toker, Peptide Bond Formation in the Protonated Serine Dimer Following Vacuum UV Photon-Induced Excitation, *Angew. Chem.*, 2023, **135**, e2022187.
22 N. J. Green, J. Xu and J. D. Sutherland, Illuminating Life's Origins: UV Photochemistry in Abiotic Synthesis of Biomolecules, *J. Am. Chem. Soc.*, 2021, **143**, 7219–7236.

23 M. Claverie, C. McReynolds, A. Petitpas, M. Thomas and S. C. M. Fernandes, Marine-derived polymeric materials and biomimetics: An overview, *Polymers*, 2020, **12**, 1002.
24 A. Sionkowska, Photochemical stability of collagen/poly(ethylene oxide) blends, *J. Photochem. Photobiol., A*, 2006, **177**, 61–67.
25 B. A. Kerwin and R. L. Remmele, Protect from light: Photodegradation and protein biologics, *J. Pharm. Sci.*, 2007, **96**, 1468–1479.
26 T. P. Cleland, C. J. Dehart, R. T. Fellers, A. J. Vannispen, J. B. Greer, R. D. LeDuc, W. R. Parker, P. M. Thomas, N. L. Kelleher and J. S. Brodbelt, High-Throughput Analysis of Intact Human Proteins Using UVPD and HCD on an Orbitrap Mass Spectrometer, *J. Proteome Res.*, 2017, **16**, 2072–2079.
27 X. Dang and N. L. Young, Ultraviolet photodissociation enhances top-down mass spectrometry as demonstrated on green fluorescent protein variants, *Proteomics*, 2014, **14**, 1128–1129.
28 S. Soorkia, C. Jouvet and G. Grégoire, UV Photoinduced Dynamics of Conformer-Resolved Aromatic Peptides, *Chem. Rev.*, 2020, **120**, 3296–3327.
29 A. Y. Pereverzev, I. Szabó, V. N. Kopysov, E. Rosta and O. V. Boyarkin, Gas-phase structures reflect the pain-relief potency of enkephalin peptides, *Phys. Chem. Chem. Phys.*, 2019, **21**, 22700–22703.
30 J. S. Brodbelt, L. J. Morrison and I. Santos, Ultraviolet Photodissociation Mass Spectrometry for Analysis of Biological Molecules, *Chem. Rev.*, 2020, **120**, 3328–3380.
31 R. Parthasarathi, Y. He, J. P. Reilly and K. Raghavachari, New insights into the vacuum UV photodissociation of peptides, *J. Am. Chem. Soc.*, 2010, **132**, 1606–1610.
32 F. Canon, A. R. Milosavljević, L. Nahon and A. Giuliani, Action spectroscopy of a protonated peptide in the ultraviolet range, *Phys. Chem. Chem. Phys.*, 2015, **17**, 25725–25733.
33 S. Bari, O. Gonzalez-Magaña, G. Reitsma, J. Werner, S. Schippers, R. Hoekstra and T. Schlathölter, Photodissociation of protonated leucine-enkephalin in the VUV range of 8-40 eV, *J. Chem. Phys.*, 2011, **134**, 024314.
34 M. L. J. Ranković, F. Canon, L. Nahon, A. Giuliani and A. R. Milosavljević, VUV action spectroscopy of protonated leucine-enkephalin peptide in the 6-14 eV range, *J. Chem. Phys.*, 2015, **143**, 244311.
35 A. Giuliani, A. R. Milosavljević, F. Canon and L. Nahon, Contribution of synchrotron radiation to photoactivation studies of biomolecular ions in the gas phase, *Mass Spectrom. Rev.*, 2014, **33**, 424–441.
36 A. R. Milosavljević, V. Z. Cerovski, M. L. Ranković, F. Canon, L. Nahon and A. Giuliani, VUV photofragmentation of protonated leucine-enkephalin peptide dimer below ionization energy, *Eur. Phys. J. D*, 2014, **68**, 68.
37 C. J. Shaffer, K. Slováková and F. Tureček, Near-UV photodissociation of phosphopeptide cation-radicals, *Int. J. Mass Spectrom.*, 2015, **390**, 71–80.
38 C. Dehon, S. Soorkia, M. Pedrazzani, C. Jouvet, M. Barat, J. A. Fayeton and B. Lucas, Photofragmentation at 263 nm of small peptides containing tyrosine: The role of the charge transfer on CO, *Phys. Chem. Chem. Phys.*, 2013, **15**, 8779–8788.
39 N. S. True, Effects of rapid intramolecular vibrational redistribution on molecular spectra at microwave frequencies, *Chem. Phys. Lett.*, 1983, **101**, 326–330.
40 R. R. Julian, The Mechanism Behind Top-Down UVPD Experiments: Making Sense of Apparent Contradictions, *J. Am. Soc. Mass Spectrom.*, 2017, **28**, 1823–1826.
41 D. Milesevic, D. Popat, P. Robertson and C. Vallance, Photodissociation dynamics of N,N-dimethylformamide at 225 nm and 245 nm, *Phys. Chem. Chem. Phys.*, 2022, **24**, 28343–28352.
42 I. Antol, M. Eckert-Maksić, M. Barbatti and H. Lischka, Simulation of the photodeactivation of formamide in the nO–π and π–π* states: An *ab initio* on-the-fly surface-hopping dynamics study, *J. Chem. Phys.*, 2007, **127**, 234303.
43 G. Féraud, M. Broquier, C. Dedonder, C. Jouvet, G. Grégoire and S. Soorkia, Excited State Dynamics of Protonated Phenylalanine and Tyrosine: Photo-Induced Reactions Following Electronic Excitation, *J. Phys. Chem. A*, 2015, **119**, 5914–5924.
44 T. N. V. Karsili, A. M. Wenge, S. J. Harris, D. Murdock, J. N. Harvey, R. N. Dixon and M. N. R. Ashfold, O-H bond fission in 4-substituted phenols: S1 state predissociation viewed in a Hammett-like framework, *Chem. Sci.*, 2013, **4**, 2434–2446.
45 K. Ranka, N. Zhao, L. Yu, J. F. Stanton and N. C. Polfer, Radical Rearrangement Chemistry in Ultraviolet Photodissociation of Iodotyrosine Systems: Insights from Metastable Dissociation, Infrared Ion Spectroscopy, and Reaction Pathway Calculations, *J. Am. Soc. Mass Spectrom.*, 2018, **29**, 1791–1801.
46 J. Dezalay, M. Broquier, S. Soorkia, K. Hirata, S. I. Ishiuchi, M. Fujii and G. Grégoire, Excited-state proton transfer in protonated adrenaline revealed by cryogenic UV photodissociation spectroscopy, *Phys. Chem. Chem. Phys.*, 2020, **22**, 11498–11507.
47 M. Pérot, B. Lucas, M. Barat, J. A. Fayeton and C. Jouvet, Mechanisms of UV photodissociation of small protonated peptides, *J. Phys. Chem. A*, 2010, **114**, 3147–3156.
48 J. Sztáray, A. Memboeuf, L. Drahos and K. Vékey, Leucine enkephalin - A mass spectrometry standard, *Mass Spectrom. Rev.*, 2011, **30**, 298–320.
49 S. Dörner, L. Schwob, K. Schubert, M. Girod, L. MacAleese, C. L. Pieterse, T. Schlathölter, S. Techert and S. Bari, The influence of the methionine residue on the dissociation mechanisms of photoionized methionine-enkephalin probed by VUV action spectroscopy, *Eur. Phys. J. D*, 2021, **75**, 142.
50 T. Tabarin, R. Antoine, M. Broyer and P. Dugourd, Specific photodissociation of peptides with multi-stage mass spectrometry, *Rapid Commun. Mass Spectrom.*, 2005, **19**, 2883–2892.
51 A. Herburger, C. Van Der Linde and M. K. Beyer, Photodissociation spectroscopy of protonated leucine enkephalin, *Phys. Chem. Chem. Phys.*, 2017, **19**, 10786–10795.

52 A. R. Milosavljević, C. Nicolas, J. Lemaire, C. Dehon, R. Thissen, J. M. Bizau, M. Réfrégiers, L. Nahon and A. Giuliani, Photoionization of a protein isolated in vacuo, *Phys. Chem. Chem. Phys.*, 2011, **13**, 15432–15436.

53 A. R. Milosavljević, C. Nicolas, J. F. Gil, F. Canon, M. Réfrégiers, L. Nahon and A. Giuliani, VUV synchrotron radiation: A new activation technique for tandem mass spectrometry, *J. Synchrotron Radiat.*, 2012, **19**, 174–178.

54 L. Nahon, N. De Oliveira, G. A. Garcia, J. F. Gil, B. Pilette, O. Marcouillé, B. Lagarde and F. Polack, DESIRS: A state-of-the-art VUV beamline featuring high resolution and variable polarization for spectroscopy and dichroism at SOLEIL, *J. Synchrotron Radiat.*, 2012, **19**, 508–520.

55 A. R. Milosavljević, C. Nicolas, J. F. Gil, F. Canon, M. Réfrégiers, L. Nahon and A. Giuliani, *Nucl. Instrum. Methods Phys. Res., Sect. B*, 2012, **279**, 34–36.

56 T. Yanai, D. P. Tew and N. C. Handy, A new hybrid exchange-correlation functional using the Coulomb-attenuating method (CAM-B3LYP), *Chem. Phys. Lett.*, 2004, **393**, 51–57.

57 T. Körzdörfer and J. L. Brédas, Organic electronic materials: Recent advances in the dft description of the ground and excited states using tuned range-separated hybrid functionals, *Acc. Chem. Res.*, 2014, **47**, 3284–3291.

58 C. Adamo and D. Jacquemin, The calculations of excited-state properties with time-dependent density functional theory, *Chem. Soc. Rev.*, 2013, **42**, 845–856.

59 F. J. A. Ferrer, J. Cerezo, E. Stendardo, R. Improta and F. Santoro, Insights for an accurate comparison of computational data to experimental absorption and emission spectra: Beyond the vertical transition approximation, *J. Chem. Theory Comput.*, 2013, **6**, 2072–2082.

60 M. J. Frisch, G. W. Trucks, H. B. Schlegel, G. E. Scuseria, M. A. Robb, J. R. Cheeseman, G. Scalmani, V. Barone, G. A. Petersson, H. Nakatsuji, X. Li, M. Caricato, A. V. Marenich, J. Bloino, B. G. Janesko, R. Gomperts, B. Mennucci, H. P. Hratchian, J. V. Ortiz, A. F. Izmaylov, J. L. Sonnenberg, D. Williams-Young, F. Ding, F. Lipparini, F. Egidi, J. Goings, B. Peng, A. Petrone, T. Henderson, D. Ranasinghe, V. G. Zakrzewski, J. Gao, N. Rega, G. Zheng, W. Liang, M. Hada, M. Ehara, K. Toyota, R. Fukuda, J. Hasegawa, M. Ishida, T. Nakajima, Y. Honda, O. Kitao, H. Nakai, T. Vreven, K. Throssell, J. A. Montgomery Jr., J. E. Peralta, F. Ogliaro, M. J. Bearpark, J. J. Heyd, E. N. Brothers, K. N. Kudin, V. N. Staroverov, T. A. Keith, R. Kobayashi, J. Normand, K. Raghavachari, A. P. Rendell, J. C. Burant, S. S. Iyengar, J. Tomasi, M. Cossi, J. M. Millam, M. Klene, C. Adamo, R. Cammi, J. W. Ochterski, R. L. Martin, K. Morokuma, O. Farkas, J. B. Foresman, M. J. Frisch and D. J. Fox, *Gaussian, 16, Revision A.03*, Gaussian Inc., Wallingford CT, 2016.

61 E. R. Johnson, S. Keinan, P. Mori-Sánchez, J. Contreras-García, A. J. Cohen and W. Yang, Revealing noncovalent interactions, *J. Am. Chem. Soc.*, 2010, **132**, 6498–6506.

62 J. Contreras-García, E. R. Johnson, S. Keinan, R. Chaudret, J. P. Piquemal, D. N. Beratan and W. Yang, NCIPLOT: A program for plotting noncovalent interaction regions, *J. Chem. Theory Comput.*, 2011, **7**, 625–632.

63 K. Biemann, Sequencing of peptides by tandem mass spectrometry and high-energy collision-induced dissociation, *Methods Enzymol.*, 1990, **193**, 455–479.

64 N. L. Burke, J. G. Redwine, J. C. Dean, S. A. McLuckey and T. S. Zwier, UV and IR spectroscopy of cold protonated leucine enkephalin, *Int. J. Mass Spectrom.*, 2015, **378**, 196–205.

65 C. M. Tseng, M. F. Lin, Y. L. Yang, Y. C. Ho, C. K. Ni and J. L. Chang, Photostability of amino acids: Photodissociation dynamics of phenylalanine chromophores, *Phys. Chem. Chem. Phys.*, 2010, **12**, 4989–4995.

66 S. Soorkia, C. Dehon, S. K. S, M. Pérot-Taillandier, B. Lucas, C. Jouvet, M. Barat and J. A. Fayeton, Ion-induced dipole interactions and fragmentation times: C_α–C_β chromophore bond dissociation channel, *J. Phys. Chem. Lett.*, 2015, **6**, 2070–2074.

67 C.-M. Tseng, M.-F. Lin, Y. L. Yang, Y. C. Ho, C.-K. Ni and J.-L. Chang, Photostability of amino acids: photodissociation dynamics of phenylalanine chromophores, *Phys. Chem. Chem. Phys.*, 2010, **12**, 4989.

68 A. V. Zabuga, M. Z. Kamrath, O. V. Boyarkin and T. R. Rizzo, Fragmentation mechanism of UV-excited peptides in the gas phase, *J. Chem. Phys.*, 2014, **141**, 154309.

69 X. Gao, S. Bai, D. Fazzi, T. Niehaus, M. Barbatti and W. Thiel, Evaluation of Spin-Orbit Couplings with Linear-Response Time-Dependent Density Functional Methods, *J. Chem. Theory Comput.*, 2017, **13**, 515–524.

70 A. R. Dongré, J. L. Jones, Á. Somogyi and V. H. Wysocki, Influence of peptide composition, gas-phase basicity, and chemical modification on fragmentation efficiency: Evidence for the mobile proton model, *J. Am. Chem. Soc.*, 1996, **118**, 8365–8374.

71 H. Wako, S. I. Ishiuchi, D. Kato, G. Féraud, C. Dedonder-Lardeux, C. Jouvet and M. Fujii, A conformational study of protonated noradrenaline by UV-UV and IR dip double resonance laser spectroscopy combined with an electrospray and a cold ion trap method, *Phys. Chem. Chem. Phys.*, 2017, **19**, 10777–10785.

72 G. Grégoire, C. Jouvet, C. Dedonder and A. L. Sobolewski, Ab initio Study of the Excited-State Deactivation Pathways of Protonated Tryptophan and Tyrosine, *J. Am. Chem. Soc.*, 2007, **129**, 6223–6231.

73 A. L. Sobolewski, W. Domcke, C. Dedonder-Lardeux and C. Jouvet, Excited-state hydrogen detachment and hydrogen transfer driven by repulsive 1π–σ^* states: A new paradigm for nonradiative decay in aromatic biomolecules, *Phys. Chem. Chem. Phys.*, 2002, **4**, 1093–1100.

74 E. M. Solovyeva, A. Y. Pereverzev, M. V. Gorshkov and O. V. Boyarkin, Ultraviolet Photodissociation of Peptides: New Insight on the Mobile Proton Model, *J. Exp. Theor. Phys.*, 2020, **130**, 626–632.

75 L. A. Macias, S. N. Sipe, I. C. Santos, A. Bashyal, M. R. Mehaffey and J. S. Brodbelt, Influence of Primary Structure on Fragmentation of Native-Like Proteins by Ultraviolet Photodissociation, *J. Am. Soc. Mass Spectrom.*, 2021, **32**, 2860–2873.